Low Temperature Plasma Technology Laboratory

Time-resolved measurements of the EEDF in a helicon plasma

David D. Blackwell and Francis F. Chen

Electrical Engineering Department

LTP-905 June, 1999

Electrical Engineering Department
Los Angeles, California 90095-1594

Time-resolved measurements of the EEDF in a helicon plasma

David D. Blackwell and Francis F. Chen

Electrical Engineering Department, University of California, Los Angeles, CA 90095-1594, USA

Abstract

An energy analyzer with the capability of making fast time-resolved measurements of the instantaneous electron current in a radiofrequency plasma has been designed and constructed. This current is then reconstructed into the instantaneous I-V characteristic at opposite phases of the RF cycle. Results are shown for the helicon wave discharge under various conditions. From the first derivative of the I-V characteristic, it is observed that there is a lack of high energy electrons characteristic of strong Landau damping, suggesting that some other mechanism is responsible for the discharge's high ionization efficiency.

PACS numbers 52.50.Dg, 52.70.Ds, 52.80.Pi

that the energy of the tail could be controlled by changing the RF frequency. Molvik et al [7,8] recently used an electron energy analyzer to detect a 20 eV pulsed electron beam which was consistent with the measured phase velocity of their helicon wave. Most recently, Chen and Hershkowitz [9] measured multiple electron beams in a helicon plasma which had qualitative agreement with the measured spectrum of phase velocity.

The one common element that these experiments share is that all of the important data was obtained using electrostatic probes or similar diagnostics. Unfortunately, measurements done with such tools are often mistakenly regarded as simple and straightforward. In actuality there are often many complications that can arise which are not easily detectable which can lead to a misinterpretation of results. This is especially true for the helicon discharge, where there may exist RF fluctuations in the temperature, density, and potential. The averaging of these changes can lead to a distorted characteristic (figure 2) which looks very much like the expected result from Landau damping distortion. In the aforementioned experiments these problems are only lightly addressed; the design of diagnostics and acquisition of data is only briefly touched upon in comparison to its interpretation.

In our experience we have found the design to be the more important concern . The first attempt at a solution was the design of a narrow band high impedance probe [10]. The high impedance circuit acts as a voltage divider between the fluctuating sheath voltage and the rest of the probe circuit as shown in figure 3 (a). The probe will follow the voltage oscillations by satisfying the condition

$$\frac{1}{kT_e}\frac{Z_{sh}}{Z_{sh}+Z_c}V_{plasma}<<1 \qquad (3)$$

with Z_{sh} the sheath impedance, Z_c the probe circuit impedance, and V_{plasma} the RF fluctuating part of the plasma potential. As seen in figure 3 (b), this "compensated" probe gives very different results from an ordinary probe. On cursory analysis, the normal probe characteristic would seem to indicate a large population of fast electrons.

Although this probe was a great improvement over the simple uncompensated design, it still only addressed one problem, that of fluctuating potential. Any fluctuations in the distribution function itself would still be averaged or masked altogether. This became a greater concern after the experiments of Ellingboe et al. [11], where a strong RF modulation of an Ar^+ emission line was observed. The intensity peak was also observed to propagate along the magnetic field with a velocity close to the helicon wave phase velocity. This seemed to indicate a population of energetic electrons moving through the plasma which are accelerated during a specific phase of the wave and traveling at the wave phase velocity. To further investigate this possibility, it would be necessary to measure the instantaneous distribution function at specific phases in the RF cycle. It is to this end that we designed an energy analyzer capable of such a measurement.

Energy Analyzer Design

In a plasma with a time varying distribution function and potential, the instantaneous current to a flat surface biased at potential V with respect to the plasma potential can be written as

$$i\left(t = t_0\right) = eA\int_{-\infty}^{\infty}\int_{-\infty}^{\infty}\int_{\sqrt{\frac{-2eV_0}{m}}}^{\infty} v_{\|} f\left(v_{\|}, v_{\perp}, t = t_0\right) dv_{\|} dv_{\perp} + C_{sh}\left(V_0\right)\left.\frac{dV}{dt}\right|_{t = t_0} \qquad (4)$$

where V_0 is the potential at time $t = t_0$, and $v_{\|}$ and $v_{\perp}$ are the parallel and perpendicular components of the velocity with respect to the surface normal. The second term in this expression is due to the capacitive current generated by the time varying plasma sheath. The sheath capacitance can be derived by approximating an ion sheath thickness from the Child-Langmuir law. This capacitance is approximately [12]

$$C_{sh}(V) = en_e A_{sh}\left(\frac{2}{eM}\right)^{1/4}\sqrt{\frac{1}{9\pi j_i}}\frac{3}{4}V^{-1/4} \tag{5}$$

with A_{sh} being the sheath area and j_i the ion flux through the sheath, which in general is also a function of potential. When a probe measurement is performed, there is no means by which the observer can separate these two currents, which can have disastrous results when the second term becomes comparable to the first. Figure 4 shows a comparison of this capacitive current with the electron current in a Maxwellian plasma. The small currents from higher energy electrons are in some instances smaller than the capacitive current. It is therefore crucial to reduce this capacitive current to as small a value as possible, otherwise it could be mistaken for current from hyperthermal electrons. If it were not for this capacitive current, the instantaneous EEDF could be obtained using an ordinary Langmuir probe. The key function of the energy analyzer is to separate the electron current from this unwanted signal; in fact, this is the *only* way to do this with a probe-based diagnostic.

The principal difference between a gridded analyzer and a Langmuir probe is that the surface which actually collects the electrons in an analyzer has no plasma sheath around it. The sheath is instead formed around a discriminator grid set in front of a

collector. Since there is no sheath, the capacitive current to the collector will be reduced to the capacitive current between itself and this grid.

These considerations affect the design in two essential ways. First, the grid spacing must be small enough to shield out any plasma from passing through it. This can be guaranteed by making $l < \lambda_D$, with l the grid spacing and λ_D the plasma Debye length. The grid for our analyzer was made of 2000 lpi nickel mesh, which gives a grid spacing of about one micron. With the highest density plasmas we could produce, on the order of 10^{13} cm^{-3}, this would be about three Debye lengths at a temperature of 3 eV; but even under these conditions, we could expect that, in the retardation region at least, the grid would sufficiently block any plasma from reaching the collector. Second, the spacing between the grid and the collector must be less than any electron collision length to ensure that the electrons which pass through the grid reach the collector unimpeded, and that no ionizing collisions occur in the region between the two. This was a much easier condition to satisfy, since for our parameters all the collision lengths were a centimeter or more, while the spacing between the grid and collector was only 2 mm. The physical layout of the analyzer is shown in figure 5 (a).

The fact that the analyzer would be working in an RF environment and collecting high frequency signals required additional modifications. The discriminator grid was shunted to the grounded stainless steel housing of the analyzer with a 10 nF capacitor (C_x) to hold it at a fixed potential. This capacitor forms an impedance divider between the plasma and collector plate to suppress the capacitive current signal. This is effective for values of $C_x >> C_p$, where C_p is the plasma sheath capacitance. This was satisfied for all experimental conditions. The collector and grid were wired to the biasing and measurement circuitry with 50Ω micro coax, and the signal from the collector was terminated in a matched load. We found from past experience that this type of transmission and measurement setup gave the best frequency response. All shields were

grounded at a single point at the output of the matching circuit. Figure 5 (b) shows the electrical schematic of the analyzer.

Experimental Procedure and Results

The experimental apparatus used is the 10 cm diameter helicon plasma source which has been described in detail elsewhere [13]. It consists of a 10 cm diam cylindrical pyrex chamber 100 cm long surrounded by eight large magnetic field coils, which can supply a magnetic field in the range 350-1000 G. The RF antenna strapped to the outside of the chamber can be placed at various positions along its length. The energy analyzer was in all cases oriented with the grid perpendicular to the magnetic field. A drawing of the experimental setup is shown in figure 6.

To test the accuracy of the analyzer, an electron gun was built. The gun (fig 7 (a)) consisted of a heated tantalum filament wound in a 3 cm diam spiral and negatively biased to act as a cathode. A tungsten screen was positioned 3 mm in front of it to act as an anode. Figure 7(b) shows the electron emittance curve of the gun with the anode grounded, where the electron beam current closely follows the Child-Langmuir law. The anode was then capacitively coupled to a function generator so that the intensity and energy of the electron beam could be modulated. This apparatus was mounted on one end of the discharge chamber, with the analyzer facing it through a vacuum feedthrough from the opposite end. The discriminator grid voltage was set with a variable power supply while the collector was biased with a +300 V battery to collect electrons and repel ions.

Figure 8 shows a representative DC vacuum characteristic of the beam as measured by the analyzer. With the capacitive current eliminated, in the electron retardation region, the first derivative of this current is related to the EEDF from equation 4 by

$$f(v_{\|}) \propto \left[\frac{di}{dV}\right]_{eV=\frac{1}{2}mv_{\|}^{2}} \tag{6}$$

with $f(v_{\|})$ defined as

$$f(v_{\|}) \equiv \int_{-\infty}^{\infty}\int_{-\infty}^{\infty} f(v_{\|},v_{\perp})dv_{\perp} \tag{7}$$

Thus for an isotropic plasma this derivative represents the actual distribution of electron energy as shown in figure 8. When this beam is fired into argon gas, it creates a plasma with a distribution function similar to those previously observed for the helicon discharge [4,5,9]. Figures 9 and 10 show the evolution of this distribution function over pressure and distance of propagation from the gun. This gave us a firsthand reference for the characteristic features we would later be looking for in the helicon plasma.

With the analyzer working satisfactorily on our simple DC plasmas, the next task was to evaluate its performance in a time varying situation. A 13.56 MHz modulation signal was applied to the anode, which simulated the effect of a rapidly changing distribution function. As the anode voltage is varied, the energy and amount of electrons emitted from the filament changes. When the beam is fired into argon, the resulting plasma also has its potential modulated. We can then simulate a plasma with a changing distribution function and a changing potential. As these parameters change, the collector current will be a nonlinear mapping of the anode voltage. Figure 11(a) shows the instantaneous electron current in a weakly ionized electron gun produced plasma with the anode modulated. By varying the analyzer's grid voltage, we can record this signal at specific phase in the RF to reconstruct the current voltage characteristic at a specific time,

or equivalently, at a specific distribution function and plasma potential. Essentially we would be taking a "snapshot" of the rapidly changing characteristic. This is a logical, more detailed extension of the measurements reported on by Molvik et al [7,8], where the instantaneous current signal at one fixed grid voltage was measured.

A test of this reconstruction method was performed by first measuring the characteristics at two DC operating points, set by adjusting the filament bias. The bias was then set to the midpoint of these two voltages, and a 13.56 MHz sine wave modulation signal was fed to the anode. The peak-to-peak amplitude of the anode signal was adjusted to match the voltage difference between the two operating points. By recording the current signal to the collector at the phases of the anode signal corresponding to these extreme points and varying the grid voltage, we had snapshots that we could compare with the DC characteristics. Figure 11(b) shows that the curves reconstructed from the modulated beam almost lie on top of the curves measured under DC conditions. The same procedure was duplicated using a moderate density plasma ($n \approx 10^{11} \mathrm{cm}^{-3}$), the results of which are shown in figure 12. Again the reconstructed curves showed excellent agreement with the DC curves. For comparative purposes, measurements of the time-averaged characteristic were taken using an RF compensated Langmuir probe, as described earlier. As could be expected, this probe characteristic fell approximately between the DC curves. The electron temperature measured was slightly higher (40%); and figure 13 shows that, for a plasma with a pronounced high energy tail, the RF modulation causes these fast electrons to be preferentially suppressed in the probe characteristic. This in fact validates earlier arguments [14] that such compensated probes were unreliable diagnostics under exactly the circumstances predicted.

With testing completed, the analyzer was then used to measure the characteristics of antenna-driven plasmas. A high-bandwidth digital storage scope was synchronized to record the maximum and minimum of the current corresponding to the most negative and

most positive phases of the oscillating plasma potential, 180˚ apart. Positioned at the midpoint of the chamber was a Nagoya Type III antenna, 20 cm in length, driven by a 13.56-MHz variable-output generator capable of supplying P ≤ 1.8 kW. The plasma density was set in the range $10^{12} - 10^{13}\text{cm}^{-3}$. These are similar to the parameters used in previous experiments in which accelerated electrons were reported [4-9] and also fell below the expected breakeven density when the collisional damping frequency overtakes the maximum Landau damping frequency calculated by Chen [1] as $n_c(\text{cm}^{-3}) = 1.63 \times 10^{12} f$, which at 13.56 MHz is about $2 \times 10^{13}\text{cm}^{-3}$.

Each data point was averaged over several plasma pulses using LabVIEW software. The entire characteristic was typically 500 points and required about an hour to produce and record. The data curves were smoothed by least squares fitting consecutive intervals of the I-V characteristic to a third order polynomial. Each interval ranges over 11 data points, which was found by trial and error to be an optimum number. By shifting the interval one data point at a time, the numerical noise is reduced sufficiently so that meaningful curves of the first derivative are obtained. Figure 14(a) shows an example of the analyzer characteristic at the two opposite phases in the RF cycle. Also shown in comparison is the characteristic from a compensated Langmuir probe. All three curves indicate exponential dependence over three decades of signal level, indicative of a Maxwellian distribution with T_e between 3 and 3.5 eV.The first derivatives shown in figure 14(b) also indicate a good exponential fit over three decades. There is a slight difference (<20%) in the temperature that is obtained from these curves, which is within the statistical error found in previous measurements with Langmuir probes. The analyzer could resolve current densities down to better than 0.1 mA/cm^2, while the total bulk electron current density under typical experimental conditions was several A/cm^2. This gives energy resolution over more than three decades and was more than capable of

detecting any non-Maxwellian beams which had been previously reported to have current densities greater than 10 mA/cm^2 [4,5].

Figure 15 shows the resulting curves of $f(v_{||})$ vs. neutral gas pressure at 360 G magnetic field and the maximum RF power of 1800 W. The average parallel electron energy calculated from the average value of $E = \frac{1}{2} m v_{||}^2$ was unrealistically high, at around 5 eV. This is most likely due to two factors. First, due to its finite size the probe is not acting as an ideal planar probe, so that in fact a sampling of the perpendicular energies is included, since the probe sheath probably has a convex rather than planar shape. Second is the lack of digital bandwidth, or number of points sampled. Both of these effects produce a rounding effect of the characteristic near the plasma potential and subsequently can underestimate of the number of low energy electrons in $f(v_{||})$. For our purposes this is an unimportant point, since the high energy regions of the curves are where our attention is focused; and it is a feature of the distribution function in these regions, rather than the quantitave values of electron energy and density, with which we are concerned. Nevertheless, an electron temperature can be estimated from an exponential fit to the high energy portion of $f(v_{||})$, and the variation of pressure over a decade causes a drop of only about 1 eV. More importantly, there is the absence of any abundant number of fast electrons, in contrast to results in our beam-produced plasmas, where some deviation from a monotonically decreasing function was seen in $f(v_{||})$ even at high pressures and large distances from the gun.

The next logical parameter to change was magnetic field strength since according to theory [1] and previous experiments [15-17] this has a dramatic effect on the wave propagation, and consequently, on the distribution function due to wave coupling. Figure 16 shows the results of this variation of magnetic field over four values. There is a decided drop in electron energy in going from the unmagnetized plasma to the helicon

plasma, which is due to the fact that there is a large increase in plasma density and hence collision rate. However, again none of the curves exhibit any pronounced deviation from monotonically decreasing, quasi-Maxwellian distribution functions.

It is apparent from these sets of curves that we were not observing any significant number of fast electrons. This negative result has the following physical implication. With the detection limit of the analyzer at approximately 10^{-3} times the thermal electron current, for a 3 eV Maxwellian plasma any hot electrons not seen would have to have energy such that they satisfy the inequality $E^{1/2} exp\left(-E/kT_e\right) < 10^{-3}$. This has a solution of $E \approx 25\text{eV}$; electrons with this energy would only comprise approximately .02% of the distribution function. Now higher energy electrons would have to have even lower density in order to escape detection; in fact, the most that there could possibly be to remain undetected at any particular energy would be $1.2 \times 10^{-3} \times E^{1/2}$, with E being the electron energy. Let us say that we have the maximum number of such fast electrons all the way out to some unrealistic value such as say, 200 eV. The entire integrated contribution of all of these electrons would only increase the ionization rate by a little more than 10% over a simple Maxwellian distribution. Clearly, any Landau-accelerated, wave trapped, or other high energy electrons have a negligible contribution to the ionization rate.

Conclusions

The principal difference between this and prior work is that the diagnostic used was experimentally demonstrated to function reliably under conditions similar to the helicon discharge. Although some authors do present convincing arguments as to why their probes are trustworthy, there has been little if any empirical data to support these claims. This is largely due to the limited amount of control the experimentalist has over the discharge parameters, so that it is at least extremely difficult to empirically assess the

performance of the probes and the effects of RF fields on them, i.e., there is no null test available since large RF fields are always present. By constructing an electron gun with a modulated anode, we were able to bypass this problem, test, and debug the analyzer under controlled conditions. To the best of our knowledge, this procedure has not been carried out with any probe diagnostic in RF plasmas to date.

The second point of these measurements is that for the first time the characteristic of a helicon plasma has been measured completely free of any possible distortion from RF effects, either through changes in the probe-sheath voltage drop or changes in the distribution function itself. The curves we were able to construct are frozen snapshots of the current-voltage characteristics. No inferences or speculations need be made about the electron energy since all of the information is contained in the curves. This presents us with a much more complete picture of the thermal properties of the plasma than can be made by integrating the high energy tail only [7] or by observing the ion emission [11].

Finally, using a new diagnostic and data acquisition method, we found that our results disagreed with all previous experiments where fast electron beams *were* observed. Our measurements with the energy analyzer described in this chapter do not confirm the observations of previous experiments, nor do they lend credence to the notion of large populations of hot, non-Maxwellian electrons being present in the helicon discharge. There was also good agreement with the analyzer data and that obtained using RF compensated Langmuir probes, which is not surprising, considering that no significant change was observed in the analyzer characteristic at opposite phases of the RF cycle. Given the current resolution capabilities of the analyzer, any such hyperthermal electron beam would comprise at most 2.4×10^{-4} times the bulk electron population in our discharge. Yet on the macroscopic level in terms of power efficiency, there is negligible difference between this source and others where such beams have been reported and attributed to being the fundamental mechanism for such efficiency. In light of these

facts,, the only reasonable conclusion is that the role of power absorption through Landau damping has been exaggerated.

1. F.F. Chen, Plasma Phys. Control. Fusion **33**, 339 (1991)

2. N.A. Krall and A.W. Trivelpiece, Principles of Plasma Physics, San Francisco Press, Inc., 1986, pp 520-532

3. N.J. Fisch, Rev. Modern Phys. **59**, 175 (1987)

4. P. Zhu and R.W. Boswell, Phys. Fluids B **3**, 869 (1991)

5. P.K. Loewenhardt, B.D. Blackwell, R.W. Boswell, G.D. Conway, and S.M. Hamberger, Phys. Rev.Lett. **67**, 2792, (1991)

6. Mieno, T., Shoji, T., and Kadota, K.,, Jpn. J. Appl. Phys. **31**, 1879 (1991)

7. A.W. Molvik, A.R. Ellingboe, and T.D. Rognlien, Phys. Rev. Lett. **79**, 233 (1997)

8. A. W. Molvik, T. D. Rognlien, J. A. Byers, R. H. Cohen, A. R. Ellingboe, E. B. Hooper, H. S. McLean, B. W. Stallard, and P. A. Vitello, J. Vac. Sci. Technol. A **14**, 984 (1996)

9. R.T.S. Chen and N. Hershkowitz, Phys. Rev. Lett. **80**, 4677 (1998)

10. I.D. Sudit and F.F. Chen, Plasma Sources Sci. Technol. **3**, 162 (1994)

11. A.R. Ellingboe, R.W. Boswell, J.P. Booth, and N. Sadeghi, Phys. Plasmas **2**, 1807 (1995)

12. H.S. Butler and G.S. Kino, Phys. Fluids B **6**, 1346 (1963)

13. D.D. Blackwell and F.F. Chen, Plasma Sources Sci. Technol. **6**, 569 (1997)

14. F.F. Chen, Plasma Phys. Control. Fusion **39**, 1533 (1997)

15. A.R. Ellingboe, and R.W. Boswell, Phys. Plasmas **3**, 2797 (1996)

16. F.F. Chen and G. Chevalier, J. Vac. Sci. Technol. A **10**, 1389 (1993)

17. A. Komori, T. Shoji, K. Miyamoto, J. Kawai, and Y. Kawai, Phys. Fluids B **3**, 893 (1991)

18 D.D. Blackwell, M.S. thesis, University of California at Los Angeles (1994)

Figure Captions

Figure 1. Computed curves showing an example of the effect of Landau damping on the distribution function (a) and the corresponding probe characteristic (b). The dashed lines show the curves from an ordinary maxwellian. A small distortion (2%) around $3<u<5$ of the distribution function ((a) inset) leads to a significant change in the measured current.

Figure 2. The mechanism and result of RF distortion: (a) illustrates how the swing in voltage maps out a current with a non zero time average due to the changing functional dependence of the probe characteristic; (b) shows numerically computed characteristics for different amplitudes of RF voltage at the probe plasma junction, showing the severe distortion caused by the time averaged currents collected at different voltages.

Figure 3: A simplified circuit diagram of the compensated probe (a) and its measured characteristic compared with an undercompensated probe (b). Both curves were recorded under the same plasma conditions. The solid line represents the poorly compensated probe characteristic, which on cursory inspection would seem to have a more energetic population of electrons. Even with filters installed, it does not satisfy equation 3., and thus suffers distortion due to the oscillating sheath potential.

Figure 4: Computed plot of the ratio of capacitive current from eq. 4 to electron current for three plasma densities in units of cm^{-3} for an electron temperature of 3 eV. The measurement of energetic electrons becomes increasingly more susceptible to error as capacitive current from the oscillating sheath becomes comparable to the real electron current with increasing sheath voltage.

Figure 5. (a) Physical layout of the analyzer, shown at approximately 2X actual size. (b) Electric circuit equivalent. The grid (1) is biased with variable DC power supply (5) and shunted directly to the stainless steel housing through the capacitor C_X (3). The collector set 2 mm behind the grid is biased with a +300 V battery while another shunting capacitor (6) offers a low impedance path for the high frequency signals. To insure good shielding against unwanted stray signals and good frequency response, the collector and grid are connected to their respective biasing circuitry through copper jacketed 50Ω micro-coax, with the collector current being measured with a 50Ω scope termination.

Figure 6. Diagram of the experimental apparatus. The analyzer is positioned 20cm downstream of the antenna for RF plasma measurements.

Fig. 7. (a) Electron gun setup with modulated anode. (b) The vacuum operating characteristic of the gun in the space charge limited regime.

Figure 8. Energy analyzer collector current characteristic and the normalized first derivative of the electron beam fired into vacuum. The gun is 50 cm away with a filament bias of -52V while the DC magnetic field is 350 gauss.

Figure 9. Evolution of the beam-plasma distribution function with increasing neutral gas pressure at a distance of 5 cm from the electron gun. The gun is DC biased at -80V with the anode removed. The beam electrons, characterized by the bump, become depleted by ionizing collisions and to some extent heat the bulk plasma as pressure is increased.

Figure 10. Evolution of the beam-plasma distribution function with increasing distance from the electron gun at a neutral gas pressure of 5 mTorr. The increasing distance thermalizes the beam faster than the increasing pressure, and after 20 cm the distribution function has gone from double humped to monotonically decreasing.

Figure 11. (a) Instantaneous current to the energy analyzer due to fluctuations in plasma potential and density in a gun-produced plasma with the anode modulated. (b) Reconstructed analyzer I-V curves of the RF modulated electron beam in vacuum 180° apart in phase (solid lines), compared to the DC generated curves (dashed lines) with corresponding voltage difference.

Figure 12. Reconstructed I-V curves taken by the energy analyzer of the electron-gun-produced plasma with the anode modulated, as compared with the DC characteristics. The center curve is the non-reconstructed, time-averaged curve obtained from an RF-compensated Langmuir probe.

Figure 13. The characteristic from a RF compensated Langmuir probe taken in a gun produced plasma with a large percentage of fast electrons (dashed line). Modulating the anode at 13.56 MHz causes the shape of the characteristic to change dramatically in that the thermal portion of the two curves still infers the same bulk temperature, but with the anode modulated there appears to be a depletion of high energy electrons.

Figure 14 (a). I-V characteristics taken by the analyzer (solid lines) and a compenstaed Langmuir probe (dashed line) in a helicon plasma at 2 mTorr Ar, 1 kW, 360G, and 20cm from the antenna. The analyzer curves were reconstructed from signals at the maximum and minimum of the RF fluctuations, 180° apart.

Figure 14(b) The first derivative of the analyzer curves shown in Figure 14(a) with the voltage axis shifted to represent electron energy. The slight separation of the curves is due to a small uncertainty in the plasma potential and is left in to make the curves visually distinguishable.

Figure 15. The first derivative of the analyzer I-V characteristic vs pressure in a helicon plasma at 1800 W and 360G magnetic field 20 cm downstream from the antenna. In the higher energy thermal region (E>5eV) and beyond we can calculate from the slope an electron temperature in the range of 2-3 eV as the pressure is dropped from 60 to 5 mTorr.

Figure 16. The first derivative of the analyzer I-V characteristic vs magnetic field strength in a helicon plasma at 1800W and 2 mTorr Ar pressure 20 cm downstream from the antenna. As previously observed [18], the electron temperature inferred from the characteristic of the unmagnetized plasma gives a higher temperature, most likely due to the lower density and collision rate.

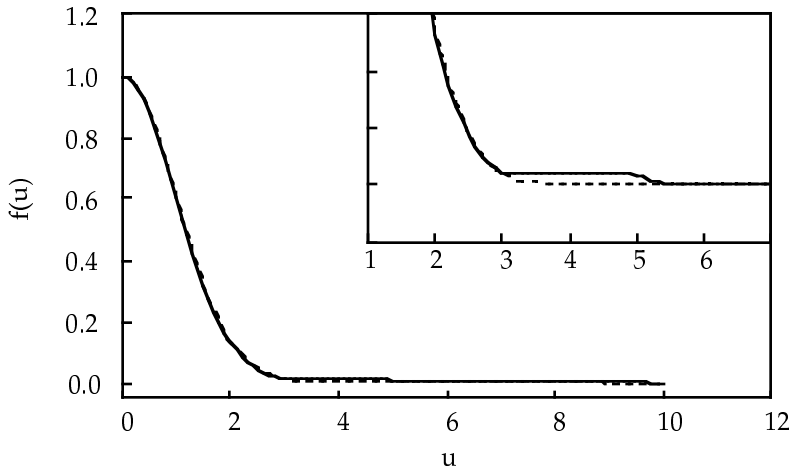
1.2
1.0
0.8
0.6
0.4
0.2
0.0
f(u)
0
2
4
6
8
10
12
u
1
2
3
4
5
6

(a)

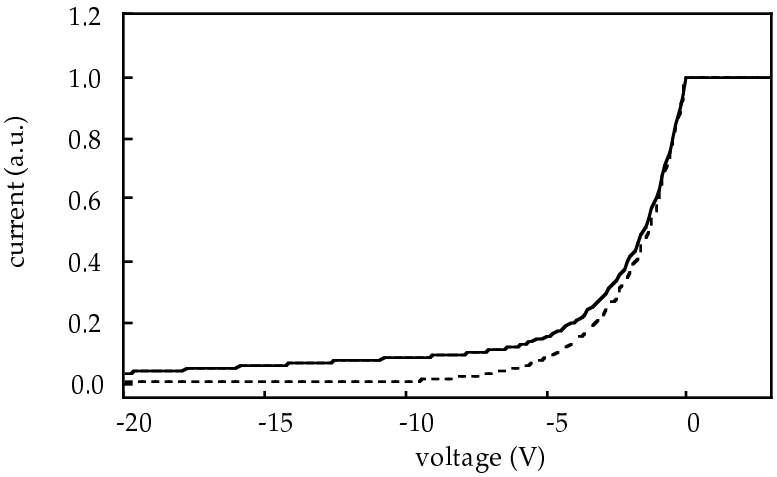
1.2
1.0
0.8
0.6
0.4
0.2
0.0
current (a.u.)
-20
-15
-10
-5
0
voltage (V)

(b)

Fig 1.

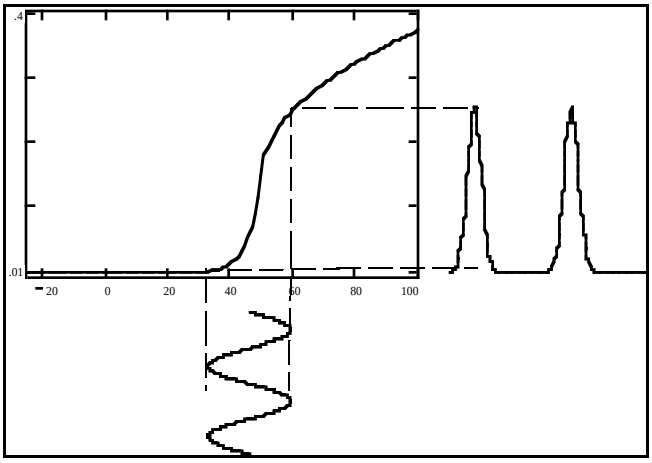
.4
.01
-20
0
20
40
60
80
100

(a)

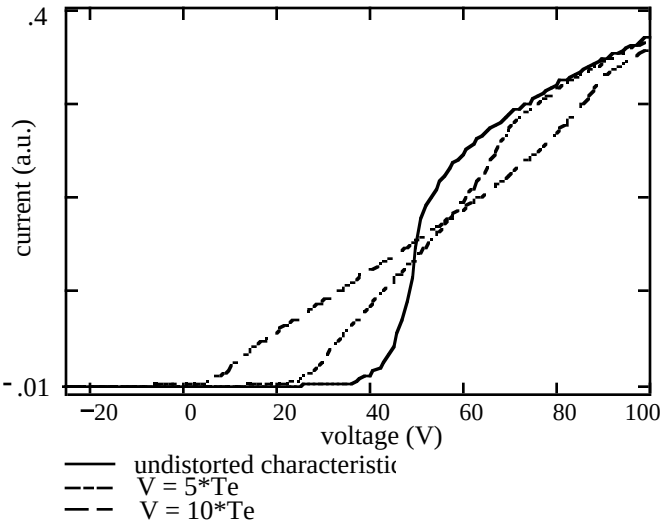
.4
current (a.u.)
.01
-20
0
20
40
60
80
100
voltage (V)
undistorted characteristic
V = 5*Te
V = 10*Te

(b)

Fig. 2

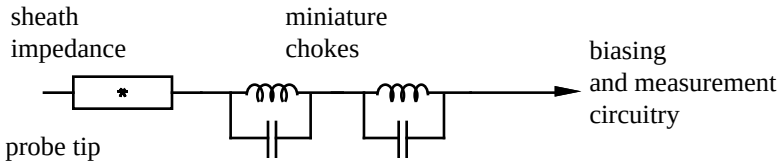
sheath
impedance
miniature
chokes
biasing
and measurement
circuitry
probe tip

(a)

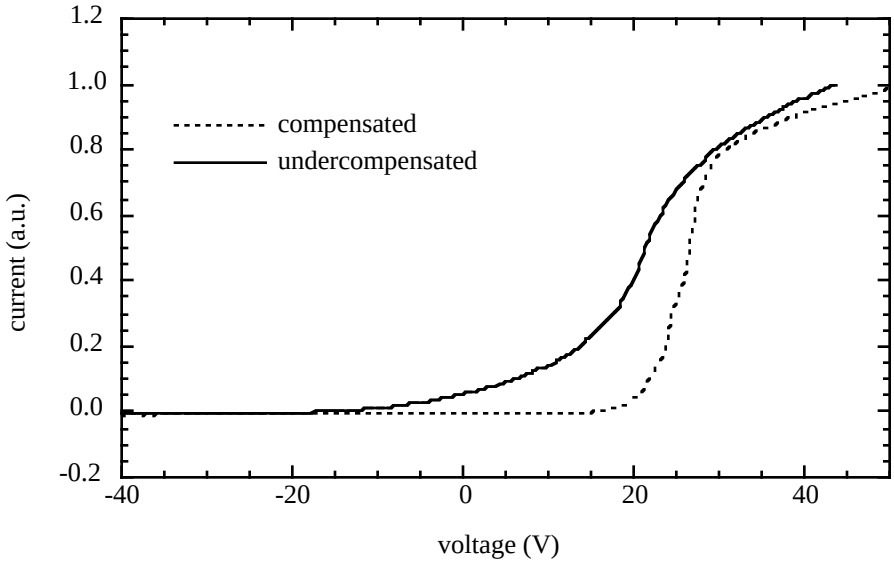
1.2
1..0
0.8
0.6
0.4
0.2
0.0
-0.2
current (a.u.)
compensated
undercompensated
-40
-20
0
20
40
voltage (V)

(b)

Fig. 3

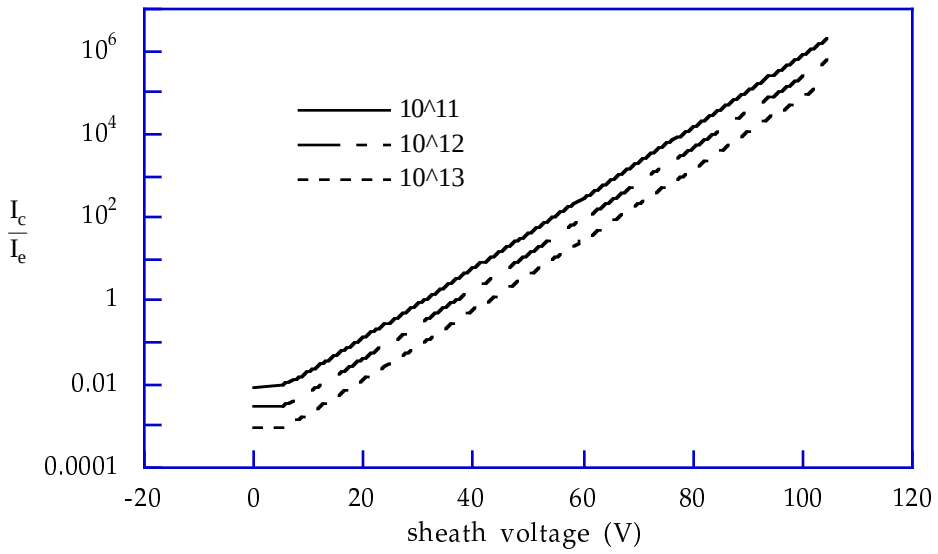
10^6
10^4
10^2
1
0.01
0.0001
$\frac{I_c}{I_e}$
10^11
10^12
10^13
-20
0
20
40
60
80
100
120
sheath voltage (V)

Fig. 4.

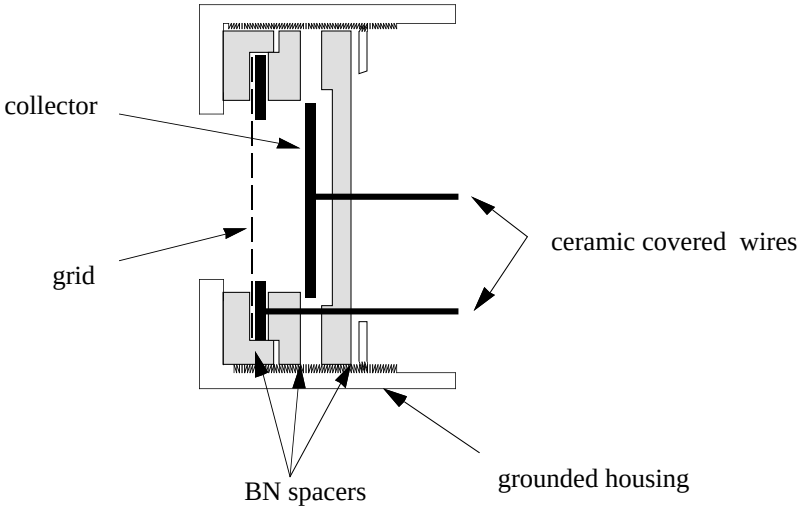
collector
grid
ceramic covered wires
BN spacers
grounded housing

(a)

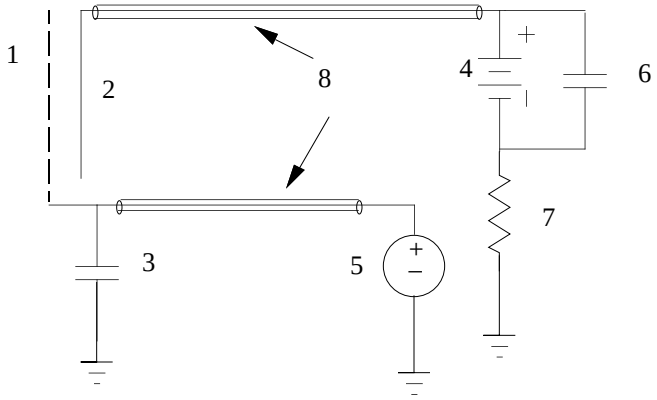
1
2
8
4
6
7
3
5
+
–

(b)

Fig. 5

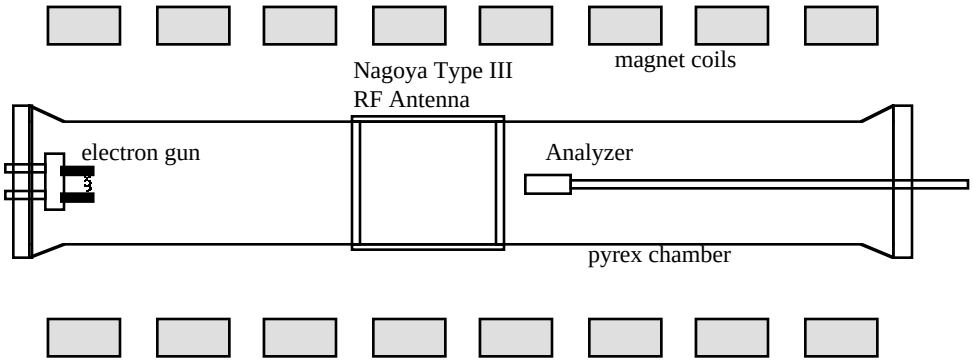
magnet coils
Nagoya Type III
RF Antenna
electron gun
Analyzer
pyrex chamber

Fig. 6

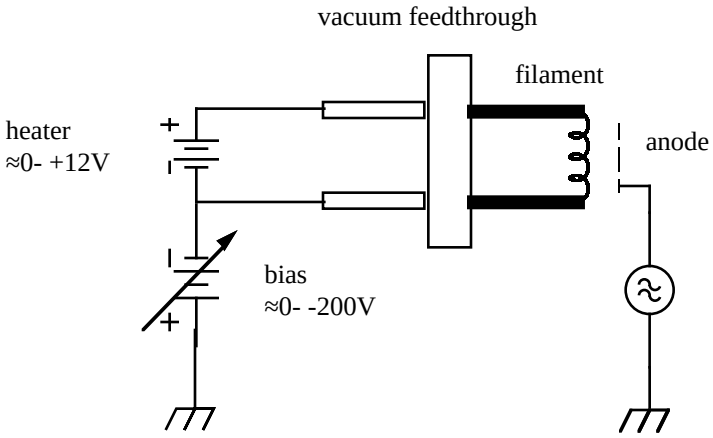
vacuum feedthrough
filament
heater
≈0- +12V
anode
bias
≈0- -200V

(a)

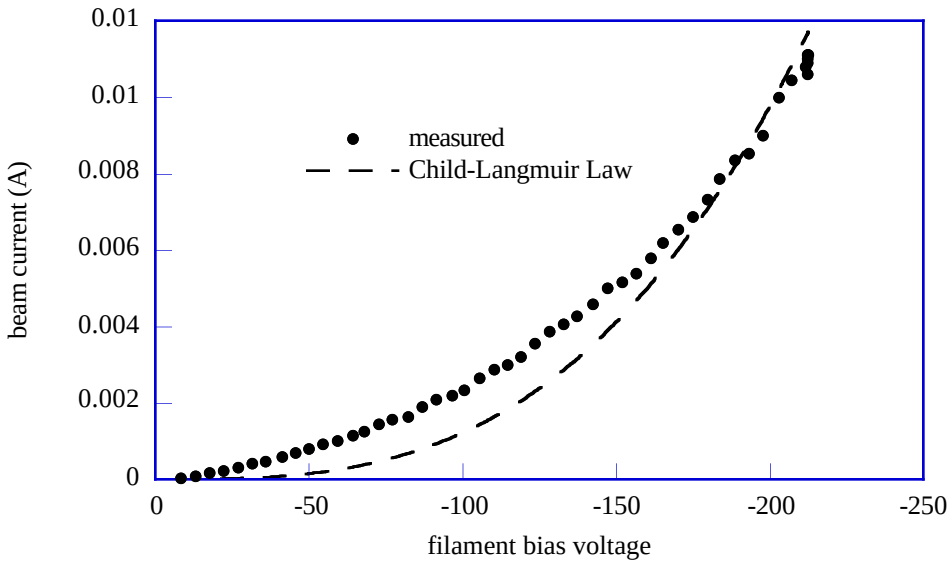
0.01
0.01
0.008
0.006
0.004
0.002
0
beam current (A)
measured
Child-Langmuir Law
0
-50
-100
-150
-200
-250
filament bias voltage

(b)

Fig. 7

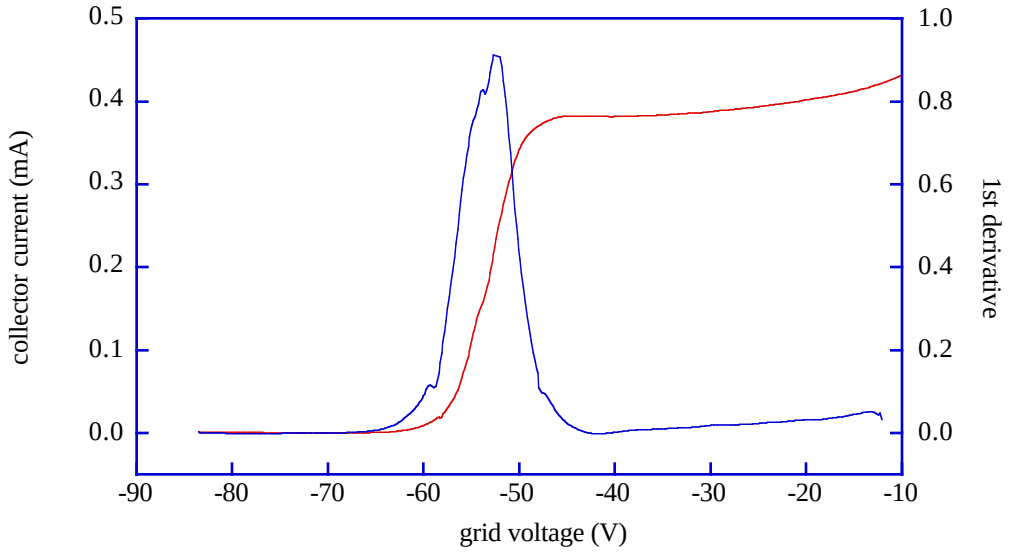
0.5
0.4
0.3
0.2
0.1
0.0
collector current (mA)
1.0
0.8
0.6
0.4
0.2
0.0
1st derivative
-90
-80
-70
-60
-50
-40
-30
-20
-10
grid voltage (V)

Fig. 8

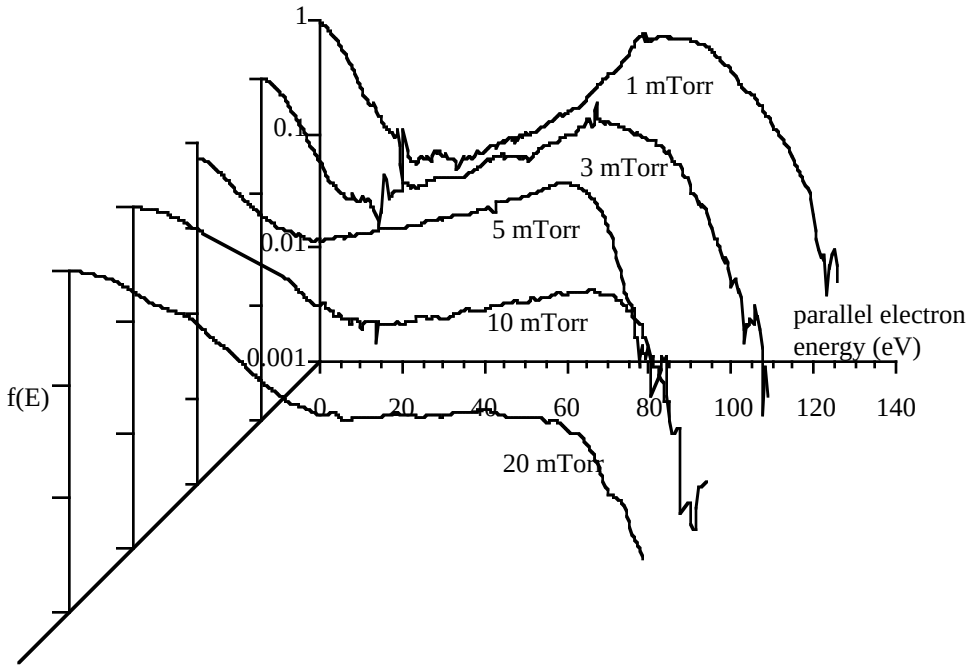
1
0.1
0.01
0.001
f(E)
1 mTorr
3 mTorr
5 mTorr
10 mTorr
20 mTorr
0
20
40
60
80
100
120
140
parallel electron
energy (eV)

Fig. 9

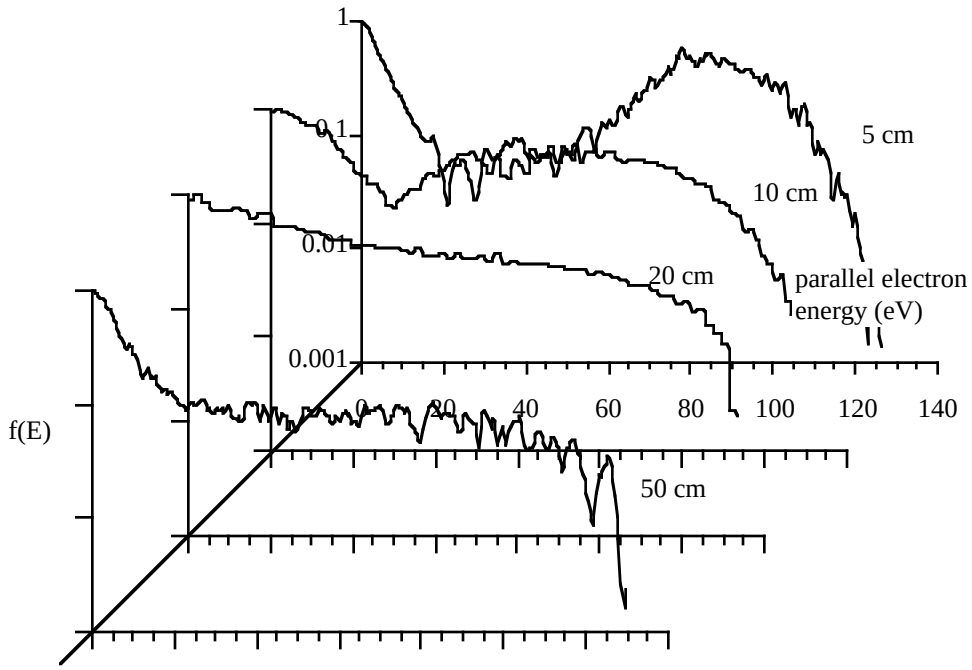
1
0.1
0.01
0.001
f(E)
0
20
40
60
80
100
120
140
5 cm
10 cm
20 cm
50 cm
parallel electron
energy (eV)

Fig. 10

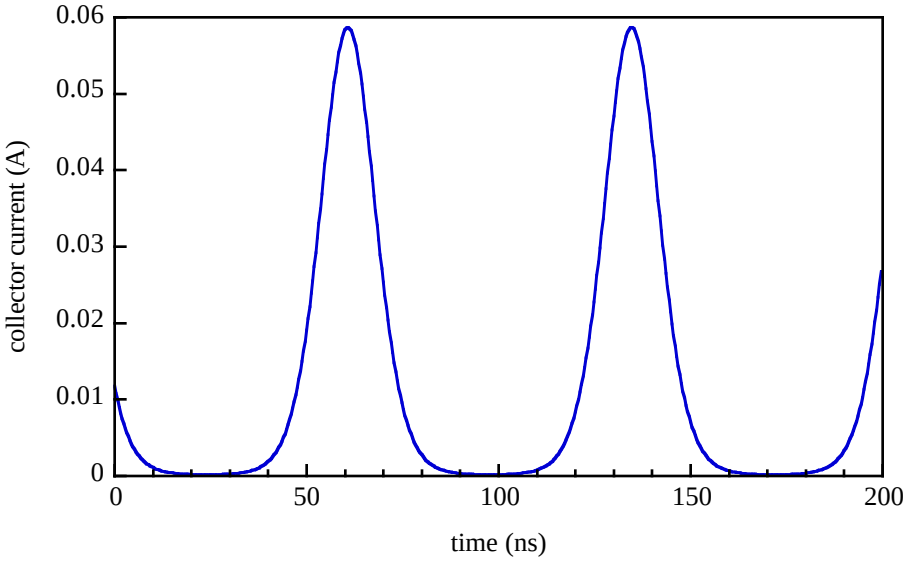
0.06
0.05
0.04
0.03
0.02
0.01
0
collector current (A)
0
50
100
150
200
time (ns)

(a)

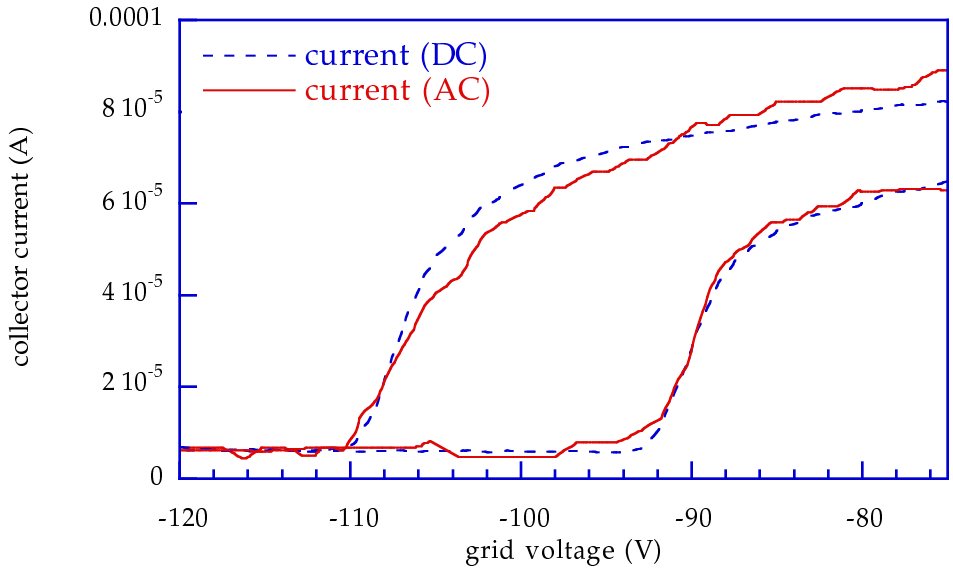
0.0001
8 10-5
6 10-5
4 10-5
2 10-5
0
collector current (A)
current (DC)
current (AC)
-120
-110
-100
-90
-80
grid voltage (V)

(b)

Fig. 11

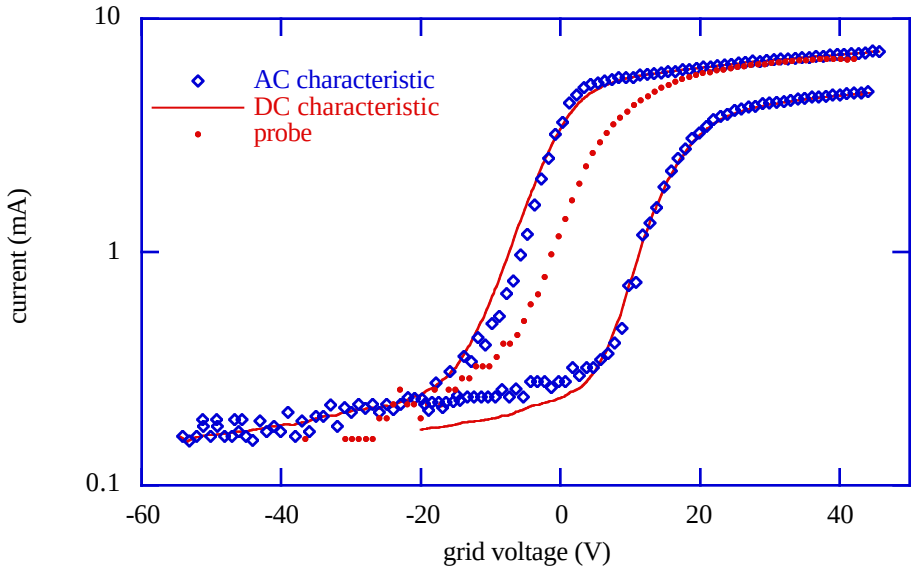
10
1
0.1
current (mA)
AC characteristic
DC characteristic
probe
-60
-40
-20
0
20
40
grid voltage (V)

Fig. 12

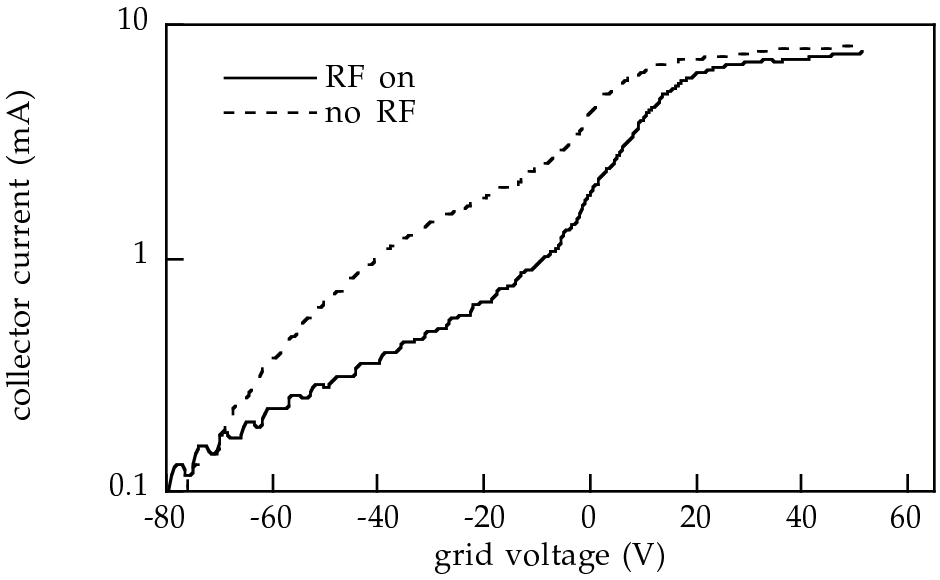
10
1
0.1
collector current (mA)
RF on
no RF
-80
-60
-40
-20
0
20
40
60
grid voltage (V)

Fig. 13

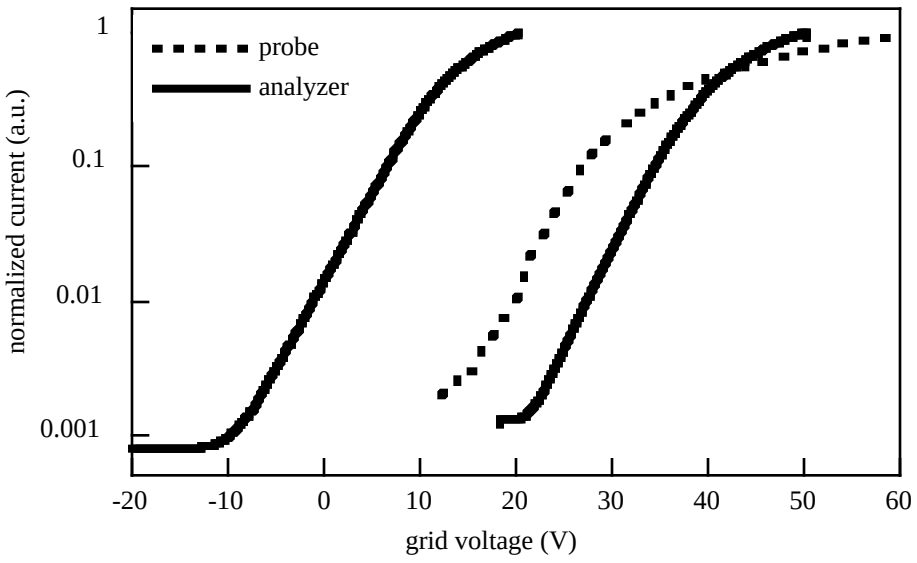
probe
analyzer
normalized current (a.u.)
1
0.1
0.01
0.001
-20
-10
0
10
20
30
40
50
60
grid voltage (V)

Fig. 14 (a)

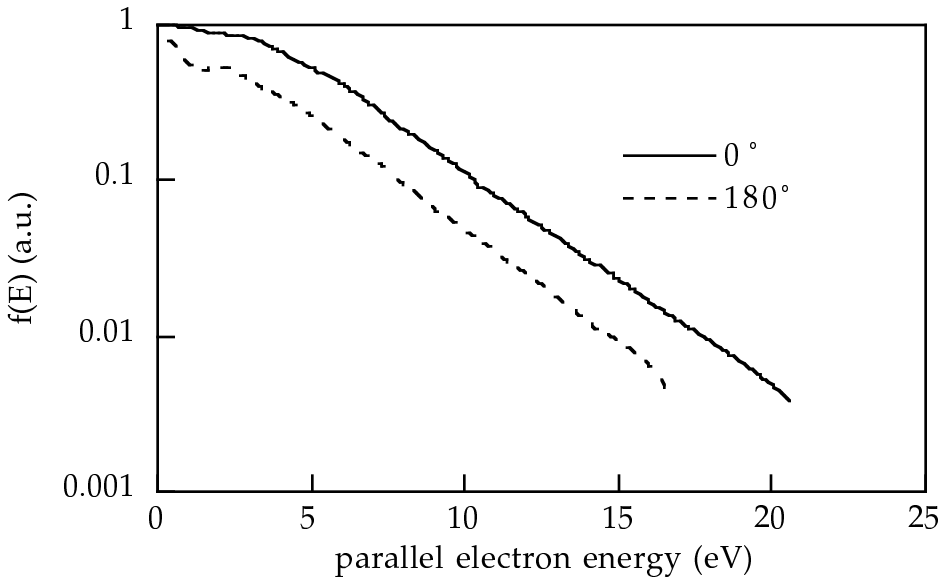
1
0.1
0.01
0.001
f(E) (a.u.)
0
5
10
15
20
25
parallel electron energy (eV)
0 °
180°

Fig. 14(b)

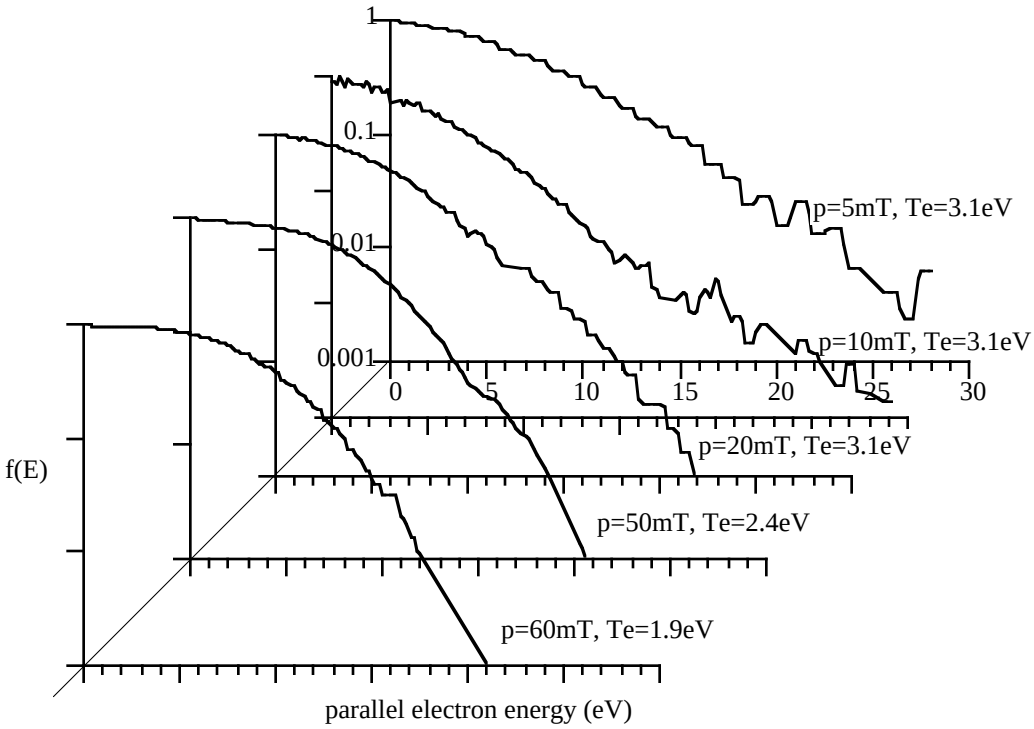
1
0.1
0.01
0.001
f(E)
0
5
10
15
20
25
30
p=5mT, Te=3.1eV
p=10mT, Te=3.1eV
p=20mT, Te=3.1eV
p=50mT, Te=2.4eV
p=60mT, Te=1.9eV
parallel electron energy (eV)

Fig. 15

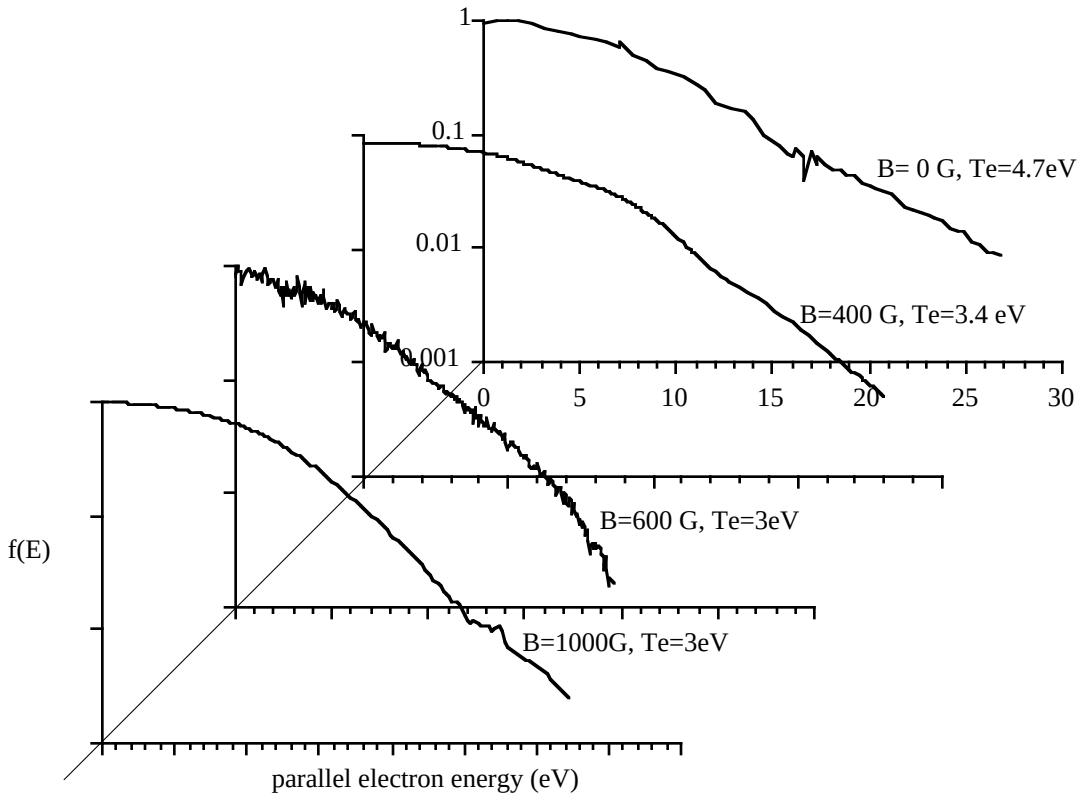
1
0.1
0.01
0.001
f(E)
0
5
10
15
20
25
30
B= 0 G, Te=4.7eV
B=400 G, Te=3.4 eV
B=600 G, Te=3eV
B=1000G, Te=3eV
parallel electron energy (eV)

Fig. 16